

Wintertime North American weather regimes and the Arctic stratospheric polar vortex

Article

Accepted Version

Lee, S. H., Furtado, J. C. and Charlton-Perez, A. J. ORCID: <https://orcid.org/0000-0001-8179-6220> (2020) Wintertime North American weather regimes and the Arctic stratospheric polar vortex. *Geophysical Research Letters*, 46 (24). pp. 14892-14900. ISSN 0094-8276 doi: <https://doi.org/10.1029/2019GL085592> Available at <https://centaur.reading.ac.uk/87746/>

It is advisable to refer to the publisher's version if you intend to cite from the work. See [Guidance on citing](#).

To link to this article DOI: <http://dx.doi.org/10.1029/2019GL085592>

Publisher: American Geophysical Union

All outputs in CentAUR are protected by Intellectual Property Rights law, including copyright law. Copyright and IPR is retained by the creators or other copyright holders. Terms and conditions for use of this material are defined in the [End User Agreement](#).

www.reading.ac.uk/centaur

CentAUR

Central Archive at the University of Reading

Reading's research outputs online

1 **Wintertime North American weather regimes and the**
2 **Arctic stratospheric polar vortex**

3 **S. H. Lee¹, J. C. Furtado², and A. J. Charlton-Perez¹**

4 ¹Department of Meteorology, University of Reading, Reading, U.K.

5 ²School of Meteorology, University of Oklahoma, Norman, Oklahoma, U.S.A.

6 **Key Points:**

- 7 • The behavior of three of four regimes over North America is significantly linked
8 to the strength of the lower-stratospheric polar vortex.
9 • A regime associated with Greenland blocking shows the strongest relationship with
10 the stratospheric polar vortex strength.
11 • The regime most strongly associated with widespread severe North American cold
12 does not show a dependency on stratospheric vortex strength.

Corresponding author: Simon Lee, s.h.lee@pgr.reading.ac.uk

Abstract

The impact of the Arctic stratospheric polar vortex on persistent weather regimes over North America is so far under-explored. Here we show the relationship between four wintertime North American weather regimes and the stratospheric vortex strength using re-analysis data. We find that the strength of the vortex significantly affects the behavior of the regimes. Whilst a regime associated with Greenland blocking is strongly favored following weak vortex events, it is not the primary regime associated with a widespread, elevated risk of extreme cold in North America. Instead, we find that the regime most strongly associated with widespread extremely cold weather does not show a strong dependency on the strength of the lower-stratospheric zonal-mean zonal winds. We also suggest that stratospheric vortex morphology may be particularly important for cold air outbreaks during this regime.

Plain Language Summary

During winter, the strength of the winds 10-50 km above the Arctic can affect the weather patterns at the surface. Generally, this influence is strongest over the North Atlantic and Europe. However, we show that the strength of stratospheric winds has a significant impact on weather patterns across North America. Our results indicate that knowledge of the stratospheric winds can provide a greater understanding of the evolution of likely weather in this region on longer time periods, including both severely cold weather (and its associated impacts on energy consumption, transport, and human health) or an unusual absence of severe cold.

1 Introduction

The behavior of the stratospheric polar vortex (SPV) is known to influence wintertime tropospheric weather patterns on subseasonal-to-seasonal (S2S) timescales (~ 15 -60 days ahead) and provide a source of predictability (e.g. Kodera & Chiba, 1995; Kolstad et al., 2010; Sigmond et al., 2013; Tripathi et al., 2015a). The variability of the SPV includes strong vortex events (Tripathi et al., 2015b) and weak vortex events, including major sudden stratospheric warmings (SSWs) (e.g. Charlton & Polvani, 2007). Whilst the mean response to an SSW or weakened SPV is a negative phase of the tropospheric Northern Annular Mode (NAM) and equatorward shift of the eddy-driven jets in the troposphere in the weeks-to-months after (Baldwin & Dunkerton, 2001; Kidston et al., 2015), there is a large amount of case-by-case and regional variability (Karpechko et al., 2017; Kretschmer et al., 2018). Weather regimes provide a helpful framework for examining stratosphere-troposphere coupling. Regimes describe the large-scale atmospheric configuration on any given day and are based on recurrent and persistent patterns in the large-scale circulation (Michelangeli et al., 1995). Because regimes exist on longer timescales than synoptic weather patterns, they provide an opportunity for longer-range prediction, useful for the energy sector (Beerli et al., 2017; Grams et al., 2017) and for the prediction of cold weather extremes in winter (Ferranti et al., 2018). Charlton-Perez et al. (2018) described the influence of the strength of the SPV on weather regimes in the North Atlantic, where the tropospheric response to changes in the stratospheric circulation is typically largest. Using four Atlantic wintertime regimes (following Cassou (2008)), they show the SPV strength significantly affects the occurrence and persistence of each regime, and the transition between regimes. This approach helps illuminate some of the reasons behind different tropospheric responses to stratospheric changes (including, but not limited to, SSWs) in a statistical sense.

Whilst the tropospheric response to changes in the SPV is more variable across North America than in the Euro-Atlantic sector, it has been implicated in driving recent extreme cold weather outbreaks in this region (so-called ‘‘polar vortex outbreaks’’ (Vaughn et al., 2017)). These are among recent billion-dollar weather and climate disasters in the

63 United States (NOAA, 2019). The North American sector is also partly influenced by
 64 Atlantic weather patterns and the NAM, which typically respond strongly to changes
 65 in the stratosphere. Kretschmer et al. (2018) used cluster analysis in the lower strato-
 66 sphere to elucidate the influence of the SPV on cold extremes in both North America
 67 and Eurasia, finding that a pattern associated with planetary wave reflection was im-
 68 portant for anomalous cold over North America. This follows earlier work by Kodera et
 69 al. (2016), who found a Pacific blocking response to SSWs dominated by planetary wave
 70 reflection, with a downstream trough over North America. In addition, the Pacific sec-
 71 tor tropospheric response to stratospheric perturbations is not necessarily of the same
 72 sign as in the Euro-Atlantic sector (Ambaum et al., 2001).

73 Although some prior work has described regimes across North America in a sim-
 74 ilar sense to the Atlantic regimes (Amini & Straus, 2019; Riddle et al., 2013; Robertson
 75 & Ghil, 1999; Straus et al., 2007; Vignaud et al., 2018), the use of regimes is not as com-
 76 mon in this region. The number of regimes and the westward and eastward extent of the
 77 region used to define the regimes varies between studies, capturing different aspects of
 78 Pacific and Atlantic variability. Moreover, the relationship between these regimes and
 79 changes in the stratospheric vortex has not yet been quantified.

80 In this article, we define four tropospheric wintertime regimes across the North Amer-
 81 ican sector and describe the relationship between the regimes and the SPV. We also in-
 82 vestigate the link between these regimes and the occurrence of extremely cold weather
 83 across North America.

84 2 Data and Methods

85 We use 00Z data from the European Centre for Medium-Range Weather Forecasts
 86 (ECMWF) ERA-Interim reanalysis (Dee et al., 2011) for all days in December–March
 87 in the period January 1979 to December 2017 (a total of 4729 days). December to March
 88 is chosen as it encompasses the period of largest SPV variability (e.g. all observed ma-
 89 jor SSWs have occurred in these months (Butler et al., 2017)). The data are re-gridded
 90 to 2.5° horizontal resolution for computational efficiency and since we are considering
 91 only large-scale features. We perform an empirical orthogonal function (EOF) decom-
 92 position of linearly de-trended 500 hPa geopotential height anomalies (with respect to
 93 the daily January 1979–December 2017 climatology) in the sector 180–30°W, 20–80°N
 94 (Figure S1). This region is chosen to include the Pacific jet exit region and include rel-
 95 evant North Atlantic variability. De-trending is performed to account for the climate change
 96 signal, although it does not notably alter the results (not shown). Data are weighted by
 97 the square-root of the cosine of latitude to give equal-area weighting in the covariance
 98 matrix. We retain the leading 12 modes of variability, which represent 80% of the to-
 99 tal variance in the 500 hPa geopotential height anomaly field. We then perform k -means
 100 clustering with $k=4$ using the Python package *scikit-learn* (Pedregosa et al., 2011). All
 101 days are then assigned to a regime based on their minimum Euclidean distance to the
 102 cluster centroids; we do not employ “no-regime” days (Grams et al., 2017). The resul-
 103 tant regimes are very similar to those found in Vignaud et al. (2018); they show these regimes
 104 are a significant representation based on the classifiability index of Michelangeli et al.
 105 (1995), so we do not repeat that calculation here. Our four regimes remain largely un-
 106 changed as a subset when five or six clusters are used, further indicating they are dom-
 107 inant patterns and form a concise characterization with reasonably large individual sam-
 108 ple sizes.

109 The probability of regime occurrence (p), which we term the occupation frequency,
 110 is given by ratio of the number of days in a given regime (n) to the total number of days
 111 (N) in the sample:

$$112 \quad p = \frac{n}{N} \quad (1)$$

113 We use 95% confidence intervals with a normal approximation to a binomial proportion
 114 confidence interval, given by:

$$115 \quad p \pm Z \sqrt{\frac{p(1-p)}{N'}} \quad (2)$$

116 where $Z = 1.96$ from the standard normal distribution. To account for the persistence
 117 of the regimes, we employ an effective sample size N' , found by using the 1-day persis-
 118 tence probability r_1 (e.g. Wilks, 2011) for each regime in each vortex state,

$$119 \quad N' = N \frac{1 - r_1}{1 + r_1} \quad (3)$$

120 We do not scale N for confidence intervals on the transition probabilities, since these are
 121 independent of the preceding regime. We define the strength of the SPV to be the ter-
 122 ticle categories of daily zonal-mean zonal wind at 100 hPa and 60°N, following Charlton-
 123 Perez et al. (2018). The 100 hPa level is chosen to represent the coupling layer between
 124 the stratosphere and troposphere and include only the effects of stratospheric pertur-
 125 bations which propagate into the lower stratosphere. The results are not qualitatively
 126 sensitive to the choice of lower-stratospheric level (not shown).

127 Statistical significance of the composite maps is determined by bootstrap re-sampling
 128 with replacement. We construct 95% confidence intervals using 50,000 re-samples per
 129 regime over all December to March days in the period 1979–2017. Random days are se-
 130 lected in blocks corresponding to the observed regime ‘events’, to test the null hypoth-
 131 esis that the composites are the result of random sub-sampling of winter days. Further
 132 detail on the bootstrapping method is provided in the Supporting Information.

133 3 Results

134 3.1 Circulation regimes

135 Composites of mean 500 hPa geopotential height anomalies for each of the four regimes
 136 are shown in Figure 1. The regimes are very similar to those defined in Straus et al. (2007)
 137 (despite a slightly different domain and analysis period) so we follow their naming con-
 138 vention. The least frequent regime (with an occupation frequency of 20%), is the Arc-
 139 tic High (ArH) regime (Figure 1a). It is associated with anomalously high geopotential
 140 heights over Greenland and the Canadian archipelago (Greenland blocking), and lower
 141 than normal geopotential heights over the Atlantic east of the United States but no sig-
 142 nificant height anomalies in the Pacific sector. The regime resembles the negative phase
 143 of the North Atlantic Oscillation (NAO–), and its occupation frequency is equivalent to
 144 the NAO– regime in Charlton-Perez et al. (2018). It is also similar to the tropospheric
 145 anomalies associated with cluster 5 in Kretschmer et al. (2018), which they associate with
 146 stratospheric planetary wave absorption. The Arctic Low (ArL) regime (Figure 1b) is
 147 not a direct counterpart of the ArH regime and is slightly more frequent (25%). Whilst
 148 the ArL regime is associated with opposite height anomalies to the ArH regime in the
 149 vicinity of Greenland and is somewhat similar to the positive NAO (NAO+), the main
 150 signature is a ridge-trough-ridge pattern extending from the Pacific across North Amer-
 151 ica, which resembles the negative phase of the Pacific–North American (PNA–) pattern.
 152 The ridge anomaly in the northeast Pacific indicates this regime is associated with a weak-
 153 ened Aleutian low and resembles a negative North Pacific Oscillation (NPO–) (Linkin
 154 & Nigam, 2008; Rogers, 1981). The Alaskan Ridge (AkR) regime (Figure 1c), occurring
 155 on 26% of days, strongly resembles the Tropical–Northern Hemisphere (TNH) pattern
 156 (Mo & Livezey, 1986) and the North American dipole (Wang et al., 2015), the latter of
 157 which was linked to the extremely cold North American winter of 2013–14. This regime
 158 is also similar to the tropospheric response to cluster 4 in Kretschmer et al. (2018), which
 159 they associate with the reflection of planetary waves by the stratosphere. We note that
 160 the AkR and ArL regimes are closest to the patterns during “polar vortex outbreaks”

161 over North America. The most frequent regime (29%) is the Pacific Trough (PT) (Fig-
 162 ure 1d), which consists of an anomalous trough centred near Alaska, and an anomalous
 163 ridge over continental North America. The trough is consistent with a positive phase of
 164 the NPO (NPO+) and the enhancement of the Aleutian Low associated with El Niño,
 165 whilst the pattern across North America resembles the positive PNA (PNA+).

166 3.2 Relationship with the stratosphere

167 To quantify the relationship between the stratospheric state and each regime, and
 168 by considering the long persistence of lower-stratospheric anomalies during winter (Fig-
 169 ure S2), we calculate the time-lagged difference in the probability of each regime between
 170 weak and strong SPV states. We calculate this difference for the 30 days before and af-
 171 ter each day in each regime, conditional on the SPV state at a zero-day lag (day 0) (Fig-
 172 ure 2). All but the AkR regime exhibit probability changes greater in magnitude than
 173 0.1, which generally peak around day 0, supporting a stratospheric influence (since this
 174 is the given state on which we condition the probability, and we would expect a near-
 175 contemporaneous regime response). The ArH regime displays the greatest difference. Its
 176 occurrence probability is 0.3–0.4 greater in a contemporaneously weak vortex versus a
 177 strong vortex; this difference exceeds 0.1 for all negative lags, which is likely influenced
 178 by the long persistence of weak SPV states (and the persistence of this regime in those
 179 conditions, c.f. Figure 3b). Moreover, for almost 20 days following a weak SPV, the prob-
 180 ability of the ArH regime is more than 0.1 greater than following a strong SPV. Con-
 181 versely, the probability of the ArL regime is around 0.1 less in the 30 days preceding a
 182 weak SPV, but this difference rapidly decays for positive lags. The PT regime becomes
 183 0.1–0.2 less likely following a weak SPV versus a strong SPV for up to 25 days; it does
 184 not display a large change in likelihood for negative lags beyond ~ 5 days.

185 Motivated by the preceding analysis, we next compute the probability of each regime
 186 given the SPV strength on the preceding day (Figure 3a). Although this is near-instantaneous,
 187 it provides a potentially useful framework for extended-range forecasting owing to the
 188 persistence and predictability of SPV strength anomalies, and the intrinsic persistence
 189 of regimes themselves. The ArH regime demonstrates the largest sensitivity to the strato-
 190 spheric state, consistent with its negative NAO-like characteristics, with an approximately
 191 linear relationship with the tercile SPV strength categories. This regime is seven times
 192 more likely following weak SPV states than strong SPV states and is the most likely regime
 193 following a weak SPV. The likelihood of the ArL regime increases with increasing SPV
 194 strength; it is approximately twice as likely following a strong versus a weak SPV. For
 195 the AkR regime, the dependency on the antecedent SPV strength is statistically insignif-
 196 icant. The PT regime is most likely following neutral and strong SPV conditions, and
 197 its behavior is generally similar to the ArL regime.

198 To further understand vortex-dependent changes in the occurrence probabilities,
 199 we compute the probability of persisting in a given regime the following day given the
 200 SPV strength on the current day (Figure 3b). The persistence of the ArH regime is most
 201 strongly dependent on the antecedent SPV strength. Its persistence decreases markedly
 202 from 0.86 following a weak SPV to 0.68 following a strong SPV, the lowest persistence
 203 probability of any of the regimes for any stratospheric state. This behavior is consistent
 204 with its similarity to NAO– (c.f. Figure 3 in Charlton-Perez et al. (2018)). None of the
 205 other three regimes exhibit significant changes in persistence probability depending on
 206 the SPV strength. Similar results are found when the total duration of each regime is
 207 stratified by the SPV strength on the day of transition into the regime (Figure S3), though
 208 this metric suggests enhanced duration of the PT regime during strong SPV conditions.

209 We also consider changes in the transitions between regimes. In Figure 3c we show
 210 the probability of transitioning from any other regime into a given regime the following
 211 day, given the SPV strength on the current day. Transitioning into the ArH regime is

2.5 times more likely during a weak SPV versus a strong SPV. The opposite is true for the ArL and PT regimes, but the relationship is slightly weaker, with the transitions approximately 50% more likely following a strong SPV versus a weak SPV. We also show the difference in specific regime transitions between a weak and a strong SPV in Table S1, but emphasize that the sample sizes are much smaller for individual transitions ($n = 38-90$, and even smaller when categorized by SPV strength), making a robust analysis difficult.

In order to discern the association between these regimes and the middle-stratospheric polar vortex (where major SSWs are commonly defined), we show the composite-mean contemporaneous 10 hPa geopotential height anomalies in Figure 4. The pattern during the ArH regime resembles a weak or displaced SPV with an anomalous wavenumber-1 configuration, consisting of anomalously high (low) geopotential heights over the central Arctic (southwest North America and northwest Europe). The anomaly pattern at 10 hPa is similar to that at 500 hPa indicating an equivalent barotropic anomaly structure. The ArL pattern is mostly opposite to ArH, with a strengthened SPV indicated by anomalously low geopotential heights over the central Arctic. The Pacific ridge anomaly present in this regime at 500 hPa does not extend to 10 hPa. The AkR regime features an anomalous wavenumber-2 splitting-type pattern with ridge anomalies in the Atlantic and Pacific, and an anomalous trough over North America. The ridge anomaly over Alaska and trough anomaly over central North America are also present at 500 hPa. The trough anomaly centred near the Hudson Bay is consistent with the similarity of this regime to the “polar vortex” outbreaks driven by a distortion to the vortex. Whilst the AkR regime does not have occurrence, persistence or transition preferences dependent on the antecedent zonal-mean zonal winds, the contemporaneous 10 hPa anomalies indicate significant disruption to the mid-stratospheric vortex. Therefore, this aspect of vortex variability may not be captured in the 100 hPa 60°N zonal-mean zonal wind; instead, the AkR regime may be more influenced by the morphology of the SPV. Additionally, the similarity of this regime to both the response to reflecting major SSWs described in Kodera et al. (2016) and the patterns found during SPV intensification in Limpasuvan et al. (2005) indicates a potential relationship with stratospheric variability. The PT regime is associated with a wavenumber-1 anomaly pattern consisting of a barotropic anomalous ridge over North America and a strengthened SPV.

3.3 Relationship with cold air outbreaks

We next assess the relationship between these regimes and the occurrence of potentially dangerous cold weather outbreaks. To do this, we calculate the probability of severe cold for each regime as the number of days in each regime with normalized 2 m temperature anomalies more than 1.5 standard deviations below the daily mean (similar to the criterion of Thompson & Wallace (2001)). This calculation is performed at each grid-point, and the result is shown in Figure 5. Corresponding maps of composite mean 2 m temperature anomalies for each regime are shown in Figure S4. Despite the large differences between the likelihood, location and extent of cold weather outbreaks in these regimes, we emphasize that all four can bring cold-weather impacts to parts of the Northern Hemisphere.

Whilst the ArH regime (Figure 5a) is the most sensitive to the stratospheric state (c.f. Figures 2 and 3), we find that it is not the most important for widespread wintertime cold weather outbreaks across North America (though there is a significant risk of severe cold (5-10%) for all but northeastern North America during this regime). Moreover, the magnitude of the mean temperature anomalies during this regime are relatively small (Figure S4a). The ArH regime is instead associated with the highest risk (>20%) of severe cold only across northwest Europe, consistent with its NAO- characteristics. We find that severe cold weather outbreaks across the continental interior of North America are most likely during the AkR regime (Figure 5c), with chances of severe cold ex-

ceeding 20%, and mean temperature anomalies widely 5°C below normal (Figure S4c). The ArL regime (Figure 5b) is associated with a 10-15% chance of extreme cold across western North America, including Alaska, whilst in the central and east of the United States there is an absence of extreme cold during this regime. The PT regime (Figure 5d) features an absence of extreme cold across most of North America, with mean temperatures widely more than 5°C above normal (Figure S4d). Extreme cold during this regime is typically confined to western Alaska and the Aleutian Islands, consistent with the western periphery of the anomalous trough. The PT regime also has the lowest overall risk of cold weather outbreaks across the Northern Hemisphere.

4 Summary and Conclusions

In this study we have shown that the behavior of three of four wintertime North American weather regimes is significantly linked to the antecedent strength of the SPV. We find that whilst the ArH regime is most sensitive to the SPV strength, it is not the most important for *widespread* extreme cold outbreaks in North America – particularly in central and northern areas where such extremes correspond to the coldest absolute temperatures. Instead, we find that the AkR regime – which does not display a significant dependence on the lower-stratospheric zonal-mean zonal wind – is associated with the greatest risk of extreme cold across most of North America. Though Figure 4c suggests a possible link exists with the state of the SPV, the similarity of this regime to the TNH pattern suggests that tropical forcing may also exhibit a large control on its behavior (e.g. Hartmann, 2015).

Further work should address the ability of sub-seasonal forecast models to correctly capture the downward coupling of stratospheric anomalies onto these regimes, as well as illuminating the dynamics involved, such as Rossby wave breaking (e.g. Michel & Rivière, 2011), and the impact of model biases. It should also be investigated whether Pacific phenomena on intra-seasonal (such as the Madden-Julian Oscillation (MJO)) to seasonal (e.g. the El Niño-Southern Oscillation (ENSO)) and decadal scales (e.g. the Pacific Decadal Oscillation (PDO)) interact constructively or destructively with the stratospheric influence.

Acknowledgments

S.H.L. was funded by the Natural Environment Research Council (NERC) via the SCENARIO Doctoral Training Partnership (NE/L002566/1). J.C.F. acknowledges funding via the National Science Foundation (NSF) Atmospheric and Geospace Sciences Program (award #AGS-1657905). The ERA-Interim reanalysis dataset is available at <https://apps.ecmwf.int/datasets/>. We acknowledge two anonymous reviewers for their detailed comments which helped improve the paper.

References

- Ambaum, M. H., Hoskins, B. J., & Stephenson, D. B. (2001). Arctic Oscillation or North Atlantic Oscillation? *Journal of Climate*, *14*(16), 3495–3507. doi: 10.1175/1520-0442(2001)014<3495:AOONAO>2.0.CO;2
- Amini, S., & Straus, D. M. (2019). Control of storminess over the Pacific and North America by circulation regimes. *Climate Dynamics*, *52*(7-8), 4749–4770. doi: 10.1007/s00382-018-4409-7
- Baldwin, M. P., & Dunkerton, T. J. (2001). Stratospheric harbingers of anomalous weather regimes. *Science*, *294*(5542), 581–584.
- Beerli, R., Wernli, H., & Grams, C. M. (2017). Does the lower stratosphere provide predictability for month-ahead wind electricity generation in Europe? *Quarterly Journal of the Royal Meteorological Society*, *143*(709), 3025–3036. doi: 10.1002/qj

- .3158
- 312 Butler, A. H., Sjoberg, J. P., Seidel, D. J., & Rosenlof, K. H. (2017). A sudden
 313 stratospheric warming compendium. *Earth System Science Data*, *9*(1), 63–76. doi:
 314 10.5194/essd-9-63-2017
- 315
- 316 Cassou, C. (2008). Intraseasonal interaction between the Madden-Julian Oscillation
 317 and the North Atlantic Oscillation. *Nature*, *455*(7212), 523–527. doi: 10.1038/
 318 nature07286
- 319 Charlton, A. J., & Polvani, L. M. (2007). A new look at stratospheric sudden warm-
 320 ings. Part I: climatology and modelling benchmarks. *Journal of Climate*, *20*(3),
 321 449–469. doi: 10.1175/JCLI3996.1
- 322 Charlton-Perez, A. J., Ferranti, L., & Lee, R. W. (2018). The influence of the strato-
 323 spheric state on North Atlantic weather regimes. *Quarterly Journal of the Royal*
 324 *Meteorological Society*, *144*(713), 1140–1151. doi: 10.1002/qj.3280
- 325 Dee, D. P., Uppala, S. M., Simmons, A. J., Berrisford, P., Poli, P., Kobayashi, S., ...
 326 Vitart, F. (2011). The ERA-Interim reanalysis: configuration and performance
 327 of the data assimilation system. *Quarterly Journal of the Royal Meteorological*
 328 *Society*, *137*(656), 553–597. doi: 10.1002/qj.828
- 329 Ferranti, L., Magnusson, L., Vitart, F., & Richardson, D. S. (2018). How far in ad-
 330 vance can we predict changes in large-scale flow leading to severe cold conditions
 331 over Europe? *Quarterly Journal of the Royal Meteorological Society*, *144*(715),
 332 1788–1802. doi: 10.1002/qj.3341
- 333 Grams, C. M., Beerli, R., Pfenninger, S., Staffell, I., & Wernli, H. (2017). Balancing
 334 Europe’s wind-power output through spatial deployment informed by weather
 335 regimes. *Nature Climate Change*, *7*(8), 557–562. doi: 10.1038/NCLIMATE3338
- 336 Hartmann, D. L. (2015). Pacific sea surface temperature and the winter of 2014.
 337 *Geophysical Research Letters*, *42*(6), 1894–1902. doi: 10.1002/2015GL063083
- 338 Karpechko, A. Y., Hitchcock, P., Peters, D. H. W., & Schneidereit, A. (2017). Pre-
 339 dictability of downward propagation of major sudden stratospheric warmings.
 340 *Quarterly Journal of the Royal Meteorological Society*, *143*(704), 1459–1470. doi:
 341 10.1002/qj.3017
- 342 Kidston, J., Scaife, A. A., Hardiman, S. C., Mitchell, D. M., Butchart, N., Bald-
 343 win, M. P., & Gray, L. J. (2015). Stratospheric influence on tropospheric jet
 344 streams, storm tracks and surface weather. *Nature Geoscience*, *8*(6), 433–440. doi:
 345 10.1038/NNGEO2424
- 346 Kodera, K., & Chiba, M. (1995). Tropospheric circulation changes associated with
 347 stratospheric sudden warmings: A case study. *Journal of Geophysical Research*,
 348 *100*(D6), 11055. doi: 10.1029/95JD00771
- 349 Kodera, K., Mukougawa, H., Maury, P., Ueda, M., & Claud, C. (2016). Absorbing
 350 and reflecting sudden stratospheric warming events and their relationship with
 351 tropospheric circulation. *Journal of Geophysical Research: Atmospheres*, *121*(1),
 352 80–94. doi: 10.1002/2015JD023359
- 353 Kolstad, E. W., Breiteig, T., & Scaife, A. A. (2010). The association between
 354 stratospheric weak polar vortex events and cold air outbreaks in the Northern
 355 Hemisphere. *Quarterly Journal of the Royal Meteorological Society*, *136*(649),
 356 886–893. doi: 10.1002/qj.620
- 357 Kretschmer, M., Cohen, J., Matthias, V., Runge, J., & Coumou, D. (2018). The dif-
 358 ferent stratospheric influence on cold-extremes in Eurasia and North America. *npj*
 359 *Climate and Atmospheric Science*, *1*(1), 44. doi: 10.1038/s41612-018-0054-4
- 360 Limpasuvan, V., Hartmann, D. L., Thompson, D. W., Jeev, K., & Yung, Y. L.
 361 (2005). Stratosphere-troposphere evolution during polar vortex intensification.
 362 *Journal of Geophysical Research*, *110*(24), 1–15. doi: 10.1029/2005JD006302
- 363 Linkin, M. E., & Nigam, S. (2008). The North Pacific Oscillation-West Pacific tele-
 364 connection pattern: Mature-phase structure and winter impacts. *Journal of Cli-*
 365 *mate*, *21*(9), 1979–1997. doi: 10.1175/2007JCLI2048.1

- 366 Michel, C., & Rivière, G. (2011). The Link between Rossby wave breakings and
 367 weather regime transitions. *Journal of the Atmospheric Sciences*, *68*(8), 1730–
 368 1748. doi: 10.1175/2011jas3635.1
- 369 Michelangeli, P.-A., Vautard, R., & Legras, B. (1995). Weather regimes: Recur-
 370 rence and quasi stationarity. *Journal of the Atmospheric Sciences*, *52*(8), 1237–
 371 1256. doi: 10.1175/1520-0469(1995)052<1237:wrraqs>2.0.co;2
- 372 Mo, K. C., & Livezey, R. E. (1986). Tropical-extratropical geopotential height tele-
 373 connections during the Northern Hemisphere winter. *Monthly Weather Review*,
 374 *114*(12), 2488–2515. doi: 10.1175/1520-0493(1986)114(2488:teghd)2.0.co;2
- 375 NOAA. (2019). *NOAA National Centers for Environmental Information (NCEI)*
 376 *U.S. Billion-Dollar Weather and Climate Disasters*. Retrieved 2019-08-01, from
 377 <https://www.ncdc.noaa.gov/billions/>
- 378 Pedregosa, F., Varoquaux, G., Gramfort, A., Michel, V., Thirion, B., Grisel, O.,
 379 ... Duchesnay, E. (2011). Scikit-learn: Machine learning in Python. *Journal of*
 380 *Machine Learning Research*, *12*, 2825–2830.
- 381 Riddle, E. E., Stoner, M. B., Johnson, N. C., L’Heureux, M. L., Collins, D. C., &
 382 Feldstein, S. B. (2013). The impact of the MJO on clusters of wintertime circu-
 383 lation anomalies over the North American region. *Climate Dynamics*, *40*(7-8),
 384 1749–1766. doi: 10.1007/s00382-012-1493-y
- 385 Robertson, A. W., & Ghil, M. (1999). Large-scale weather regimes and local climate
 386 over the western United States. *Journal of Climate*, *12*(6), 1796–1813. doi: 10
 387 .1175/1520-0442(1999)012<1796:LSWRAL>2.0.CO;2
- 388 Rogers, J. C. (1981). The North Pacific oscillation. *Journal of Climatology*, *1*(1),
 389 39–57. doi: 10.1002/joc.3370010106
- 390 Sigmond, M., Scinocca, J. F., Kharin, V. V., & Shepherd, T. G. (2013). Enhanced
 391 seasonal forecast skill following stratospheric sudden warmings. *Nature Geo-*
 392 *science*, *6*(2), 98–102. doi: 10.1038/ngeo1698
- 393 Straus, D. M., Corti, S., & Molteni, F. (2007). Circulation regimes: Chaotic variabil-
 394 ity versus SST-forced predictability. *Journal of Climate*, *20*(10), 2251–2272. doi:
 395 10.1175/JCLI4070.1
- 396 Thompson, D. W., & Wallace, J. M. (2001). Regional climate impacts of the
 397 Northern Hemisphere annular mode. *Science*, *293*, 85–89. doi: 10.1126/
 398 science.1058958
- 399 Tripathi, O. P., Baldwin, M., Charlton-Perez, A., Charron, M., Eckermann, S. D.,
 400 Gerber, E., ... Son, S. W. (2015a). The predictability of the extratropical strato-
 401 sphere on monthly time-scales and its impact on the skill of tropospheric forecasts.
 402 *Quarterly Journal of the Royal Meteorological Society*, *141*(689), 987–1003. doi:
 403 10.1002/qj.2432
- 404 Tripathi, O. P., Charlton-Perez, A., Sigmond, M., & Vitart, F. (2015b). En-
 405 hanced long-range forecast skill in boreal winter following stratospheric strong
 406 vortex conditions. *Environmental Research Letters*, *10*(10), 104007. doi:
 407 10.1088/1748-9326/10/10/104007
- 408 Vigaud, N., Robertson, A., & Tippett, M. (2018). Predictability of recurrent
 409 weather regimes over North America during winter from submonthly reforecasts.
 410 *Monthly Weather Review*, *146*(8), 2559–2577. doi: 10.1175/mwr-d-18-0058.1
- 411 Wang, S. Y. S., Huang, W. R., & Yoon, J. H. (2015). The North American win-
 412 ter ‘dipole’ and extremes activity: A CMIP5 assessment. *Atmospheric Science Let-*
 413 *ters*, *16*(3), 338–345. doi: 10.1002/asl2.565
- 414 Waugh, D. W., Sobel, A. H., & Polvani, L. M. (2017). What is the polar vortex
 415 and how does it influence weather? *Bulletin of the American Meteorological Soci-*
 416 *ety*, *98*(1), 37–44. doi: 10.1175/BAMS-D-15-00212.1
- 417 Wilks, D. (2011). *Statistical methods in the atmospheric sciences*. Academic Press.

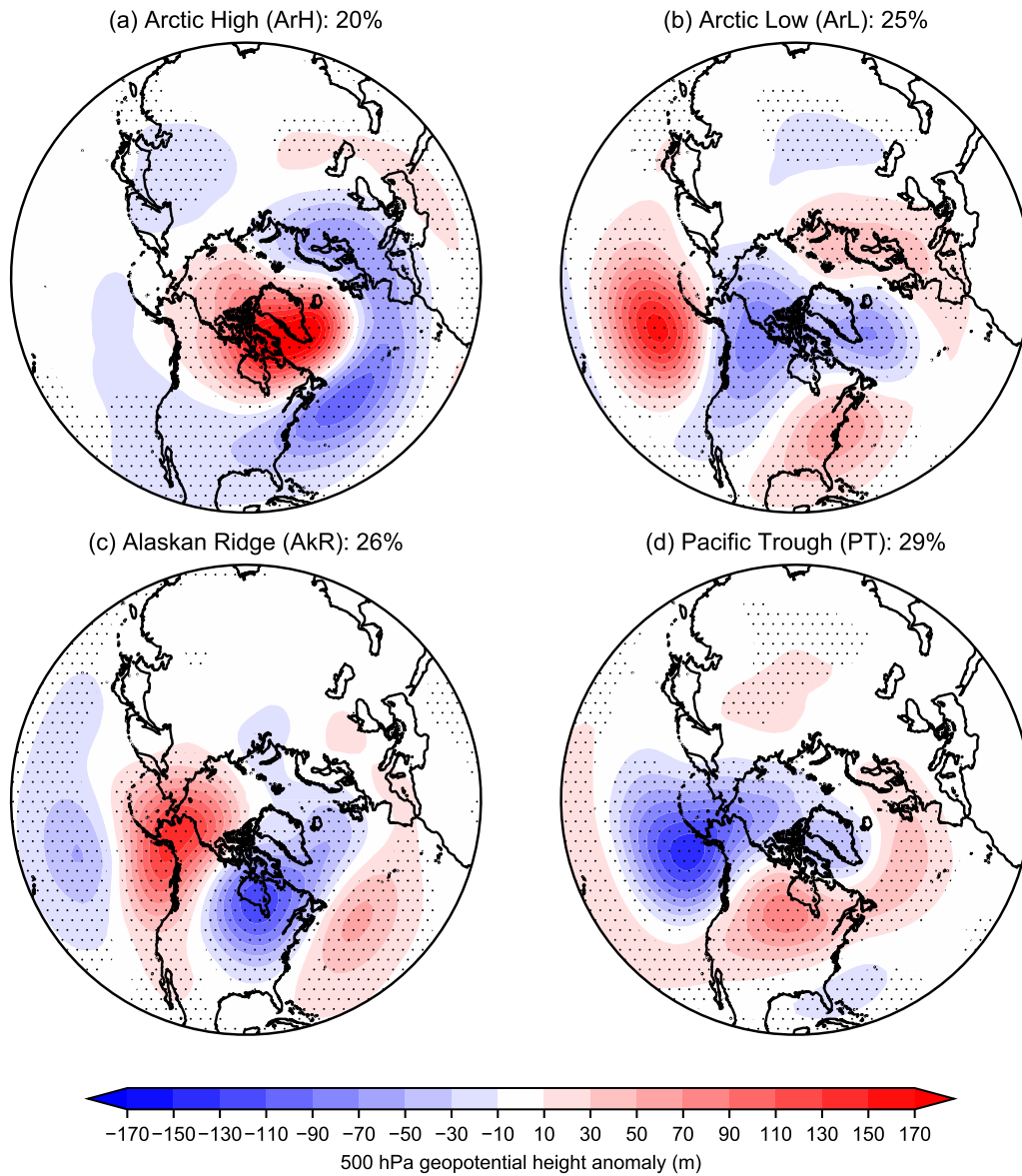


Figure 1. Composite mean 500 hPa geopotential height anomalies (meters) for each of the four regimes. Anomalies are expressed with respect to the de-trended daily January 1979–December 2017 mean. Percentages indicate the occupation frequency of the regime (the percentage of days assigned to the regime in the November–March period). Stippling indicates significance at the 95% confidence level according to a two-sided bootstrap re-sampling test.

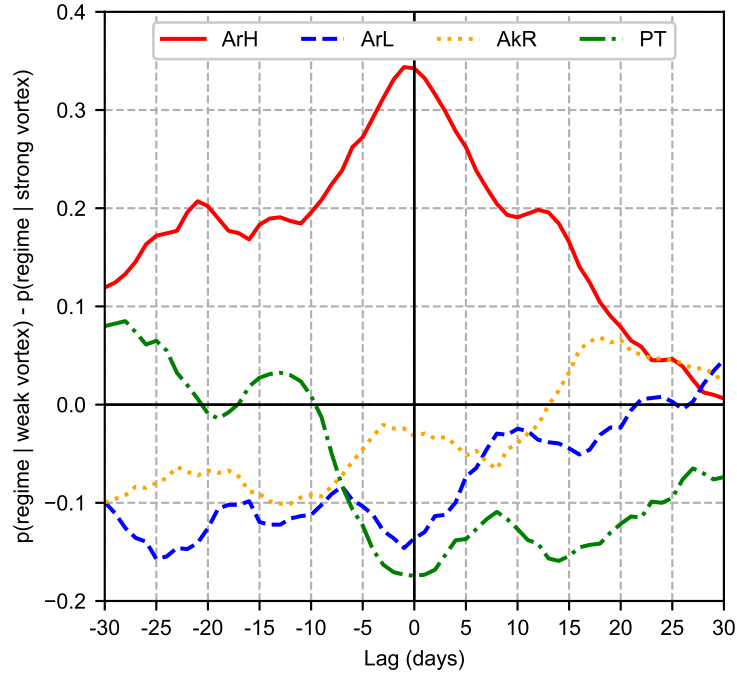


Figure 2. Difference in the occurrence probability of each regime between weak and strong stratospheric polar vortex states for -30 to +30 day lags, conditional on the vortex state at day 0.

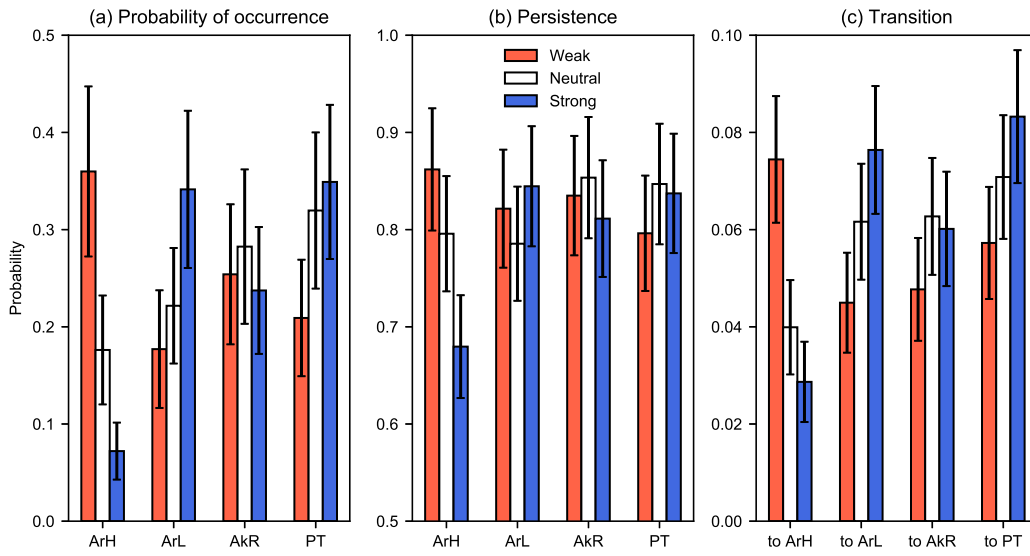


Figure 3. (a) Probability of occurrence, (b) persistence, and (c) transition of each regime given the tercile category of the stratospheric polar vortex strength on the preceding day. Error bars indicate 95% binomial proportion confidence intervals using a normal approximation (see text for details). Colors indicate the tercile category of the 100 hPa 60°N zonal-mean zonal wind based on daily January 1979–December 2017 climatology.

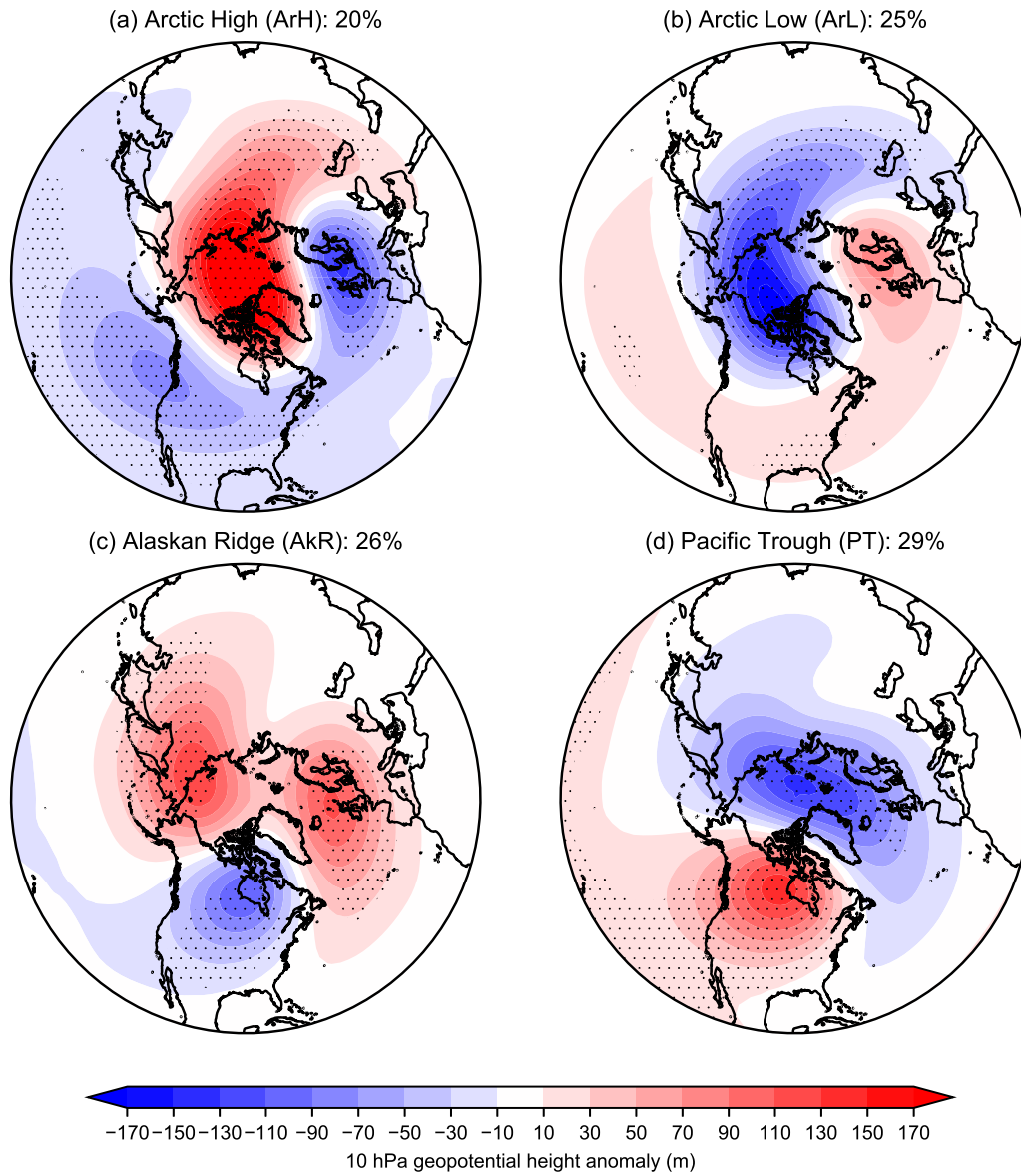


Figure 4. Composite mean 10 hPa geopotential height anomalies (meters) for days classified in each of the four regimes. Anomalies are expressed with respect to the de-trended January 1979–December 2017 mean. Stippling indicates significance at the 95% confidence level according to a two-sided bootstrap re-sampling test.

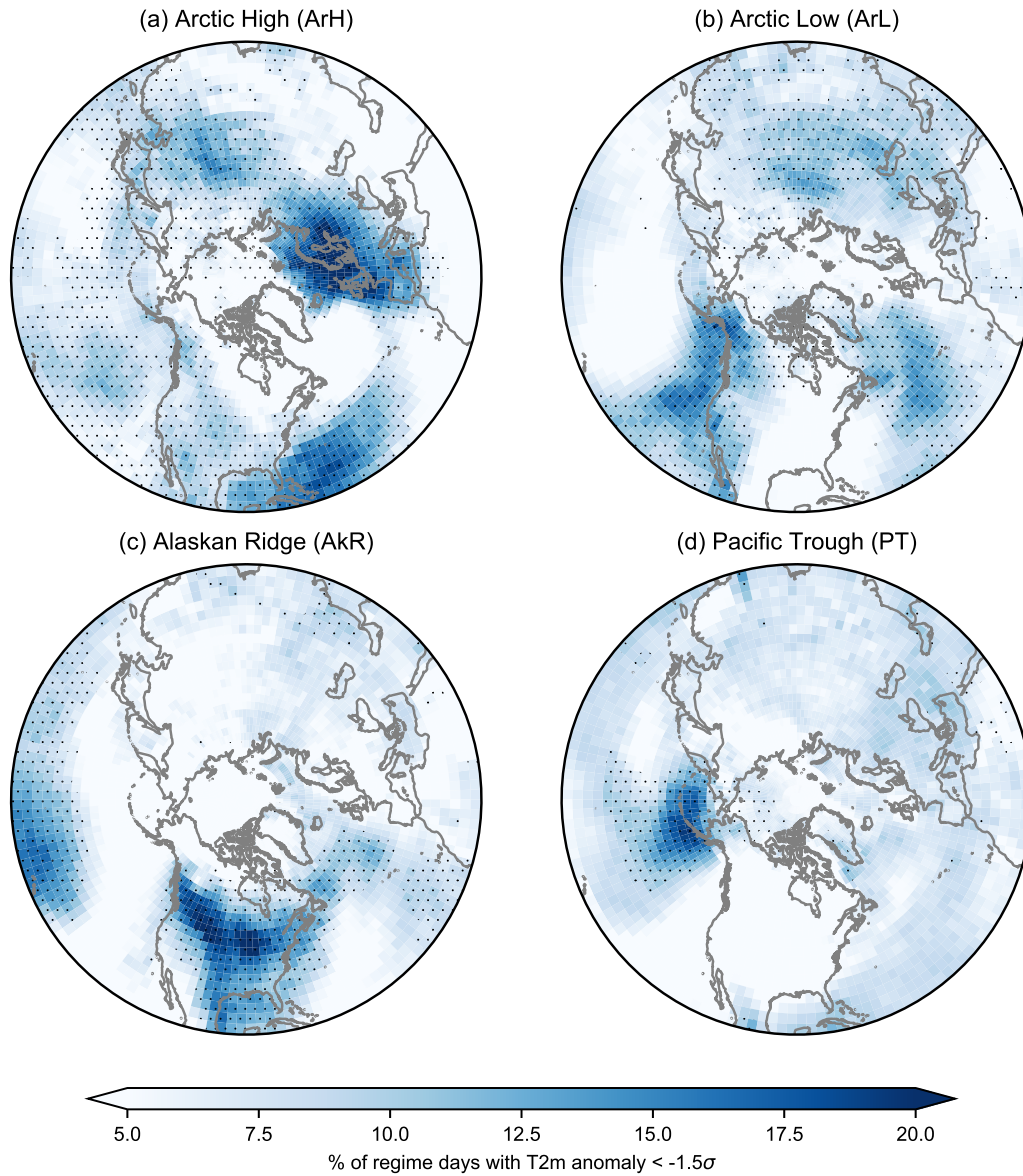


Figure 5. Percent of all days in each regime with daily standardized 2 m temperature anomalies $< -1.5\sigma$ (with respect to the linearly de-trended daily January 1979–December 2017 mean). Stippling indicates significance at the 95% confidence level according to a one-sided bootstrap re-sampling test.